Structural Analysis of the In-Vessel RMP IM-Coils of the TCABR Tokamak

André S. Bouzan, Roberto Ramos Jr., Felipe M. Salvador, Juan I. Elizondo, Joseph Y. Saab Jr., Felipe Bekman, Francisco T. Degasperi, Ruy M. O. Pauletti, and Gustavo P. Canal

***Abstract*— An upgrade of the Tokamak à Chauffage Alfvén Brésilien (TCABR) is being carried out to allow for studies of the impact of resonant magnetic perturbation (RMP) fields on plasma instabilities known as edge localized modes (ELMs). For that, a unique set of RMP coils is being designed and will be installed inside the vacuum vessel. These coils will be subject to extreme conditions: they have to operate with relatively high electric currents (≤2 kA), voltages (≤4 kV), temperatures (≤200 °C), and vacuum (≤1 × 10^{-7} mbar), to withstand strong electromagnetic forces (≤6 kN) and to be relatively small to fit the reduced space available between the vacuum vessel walls and the graphite protection tiles. This work presents a complete structural analysis of one particular set of these in-vessel coils (the so-called IM-coils) using finite element numerical simulations. The maximum equivalent von-Mises stresses obtained for the proposed mechanical design satisfies both ASME and ITER criteria.**

***Index Terms*— Edge localized modes (ELMs) control, resonant magnetic perturbation (RMP) coils, structural analysis, tokamak, Tokamak à Chauffage Alfvén Brésilien (TCABR).**

I. Introduction

THE Tokamak à Chauffage Alfvén Brésilien (TCABR) is a tokamak operated at the University of São Paulo, Brazil, that features, in its current hardware configuration, major radius $R_0 = 0.62$ m, plasma minor radius $a \leq 0.18$ m, toroidal magnetic field $B_0 \leq 1.1$ T, plasma current $I_p \leq 100$ kA, and maximum discharge duration of 100 ms [1]. TCABR will be upgraded to operate in the high confinement mode (H-mode), where new forms of instabilities, known as edge localized modes (ELMs), are expected to occur [2], [3]. These instabilities cause repetitive heat flux pulses that can be unbearable by the most advanced materials. Since relatively small, resonant magnetic perturbations (RMPs) fields have been successfully used to mitigate, or completely suppress, ELMs [4], [5], RMP coils will also be used to control ELMs in TCABR.

The main objective of the TCABR upgrade is to allow new experiments to validate ideal or visco-resistive magnetohydrodynamic (MHD) models as well as kinetic transport models in a variety of plasmas shapes, RMP field spectra, and RMP coils geometry. To allow for a variety of plasma scenarios, a new set of high-performance power supplies for plasma shape and position control are being designed [6]. This upgrade will also allow researchers to investigate the impact of RMP fields applied from both high- and low-field sides (HFS and LFS, respectively). For this, six toroidal arrays of coils will be installed inside the vacuum vessel: three arrays on the HFS (CP-coils) and three arrays on the LFS (I-coils), Fig. 1. Each one of these arrays is composed of 18 coils equally spaced in the toroidal direction. The 54 coils installed on the LFS (the I-coils) are divided into three groups: upper I-coils (IU-coils), middle I-coils (IM-coils), and lower I-coils (IL-coils). The other 54 coils installed on the HFS (the CP-coils) are also divided into three groups: upper CP-coils (CPU-coils), middle CP-coils (CPM-coils), and lower CP-coils (CPL-coils). The number of coils in each toroidal array was selected based on the number of toroidal field coils and vacuum vessel ports. Given the number of coils in the toroidal direction, these sets of coils will be able to produce toroidal mode numbers $n \leq 9$.

Besides installing RMP coils inside the vacuum vessel, additional components and new plasma diagnostics will also be installed, such as graphite protection tiles and new optical, electrostatic, and magnetic diagnostics. These new diagnostics and components do have an impact on the design of the RMP coils and must be accordingly considered. For example, as the distance between the RMP coils and the graphite protection tiles is only 1 mm, the structure that houses the coil conductors, the coil casing, must be stiff enough to prevent it from touching the tiles during operation and stay within the linear elastic regime of the material. In addition, the coil casings must not obstruct the observation ports and must allow for cable routing of plasma diagnostics and the coils themselves.

The main objective of this work is to verify if the allowable stress criteria are all satisfied by the proposed mechanical design of the IM-coils casing. To this end, the multiphysics finite element simulation software ANSYS 2022 R2 was used to calculate, using the ANSYS' Maxwell 3-D module, the

Manuscript received 3 October 2023; revised 2 February 2024; accepted 27 February 2024. This work was supported in part by the Coordenação de Aperfeiçoamento de Pessoal de Nível Superior–Brazil (CAPES) and in part by the São Paulo Research Foundation (FAPESP) under Grant #2022/04857-2. The review of this article was arranged by Senior Editor R. Chapman. *(Corresponding author: André S. Bouzan.)*

André S. Bouzan, Roberto Ramos Jr., and Ruy M. O. Pauletti are with the Polytechnic School, University of São Paulo, São Paulo 05508-010, Brazil (e-mail: andre.bouzan@usp.br).

Felipe M. Salvador, Juan I. Elizondo, and Gustavo P. Canal are with the Institute of Physics, University of São Paulo, São Paulo 05508-090, Brazil.

Joseph Y. Saab Jr. and Felipe Bekman are with the Mauá Institute of Technology, São Caetano do Sul 09580-900, Brazil.

Francisco T. Degasperi is with the Faculty of Technology, São Paulo 01101-010, Brazil.

Color versions of one or more figures in this article are available at https://doi.org/10.1109/TPS.2024.3371903.

Digital Object Identifier 10.1109/TPS.2024.3371903

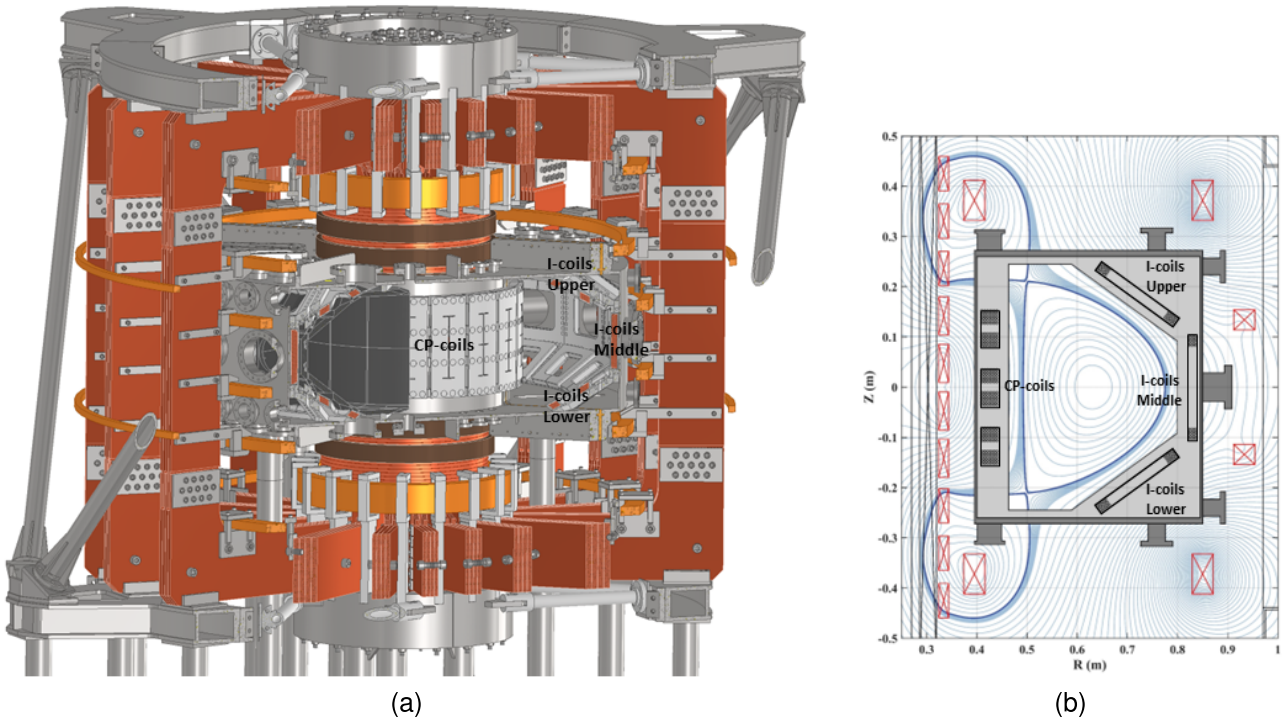

Fig. 1. (a) Three Dimensional CAD model of TCABR showing the RMP coils and graphite protection tiles. Source: Developed by A. S. Bouzan. (b) Poloidal cross section of TCABR showing a double-null plasma configuration and six RMP coils from each of the six toroidal arrays [7].

electromagnetic forces on the coil conductors and also the ohmic power losses within them. This information was then used in transient thermal simulations, using the ANSYS' transient thermal module, to calculate the time evolution of the temperature distribution within the mechanical casing and coil conductors along eight consecutive discharges. Finally, the distributed forces and temperature after the last of these eight discharges are used in a static structural simulation, using the ANSYS' static structural module, to estimate deformations and stresses in the mechanical casings.

II. Physical and Mechanical Design Descriptions

A. Physical Design Description

The conceptual/physical criteria used to guide the mechanical design of these coils came from MHD plasma simulations that focused on optimizing the number of turns of the coils and their position and orientation within the TCABR vacuum vessel [7]. This optimization process consisted of running the M3D-C^1 MHD code to obtain the coil geometry that produces the most effective RMP fields to suppress/mitigate ELMs in TCABR. M3D-C^1 is a high-order finite elements code, with C^1 continuity, that solves a set of nonlinear, two-fluid, visco-resistive MHD equations [8]. The position and orientation of the coils, relative to the plasma, were used as the starting point for the mechanical design of the coils casings.

B. Mechanical Design Description

The conceptual/physical design aforementioned defines the position of the IM-coils, their orientation relative to the plasma, their number of turns ($N = 12$), and the maximum electric current (2 kA) required to produce effective RMP fields to suppress/mitigate ELMs in TCABR. The coil conductors/wires will be made of copper and will be covered by a layer of Kapton for electrical insulation. The diameter of the copper wires was chosen to be 4 mm to avoid the conductors' temperatures to surpass the limit of 80 °C after a discharge. The wires will then be embedded in an epoxy resin, forming a package, which must be housed by the stainless-steel coil casings.

As shown in Fig. 2, the main components of the IM-coil mechanical casing are: 1) the coil cover; 2) structural bars; and 3) the base plate. These components are assembled and fastened to the straps using M8 bolts. The straps will be welded onto the wall of the vacuum vessel, the structural bars will be welded onto the coil cover, and the base plate will be fixed on the structural bars using M5 bolts. All these components will be manufactured from 316L stainless steel, which is the same used for the vacuum vessel. Fig. 2 also shows the finite element mesh used in the simulations presented here.

III. Electromagnetic Analysis

The electromagnetic forces and ohmic losses on the coil wires are obtained from numerical simulations using the ANSYS' module Maxwell 3-D. In these simulations, all the coil currents and their associated magnetic fields are constant in time. Therefore, the magnetic field can be calculated using the Biot–Savart law. The forces are caused primarily by the interaction of the coil currents with the toroidal magnetic field of the machine.

Using the periodicity of the RMP and toroidal field coils along the toroidal direction (one set of coils at every 20°), a simplified model based on a 40° toroidal span of TCABR

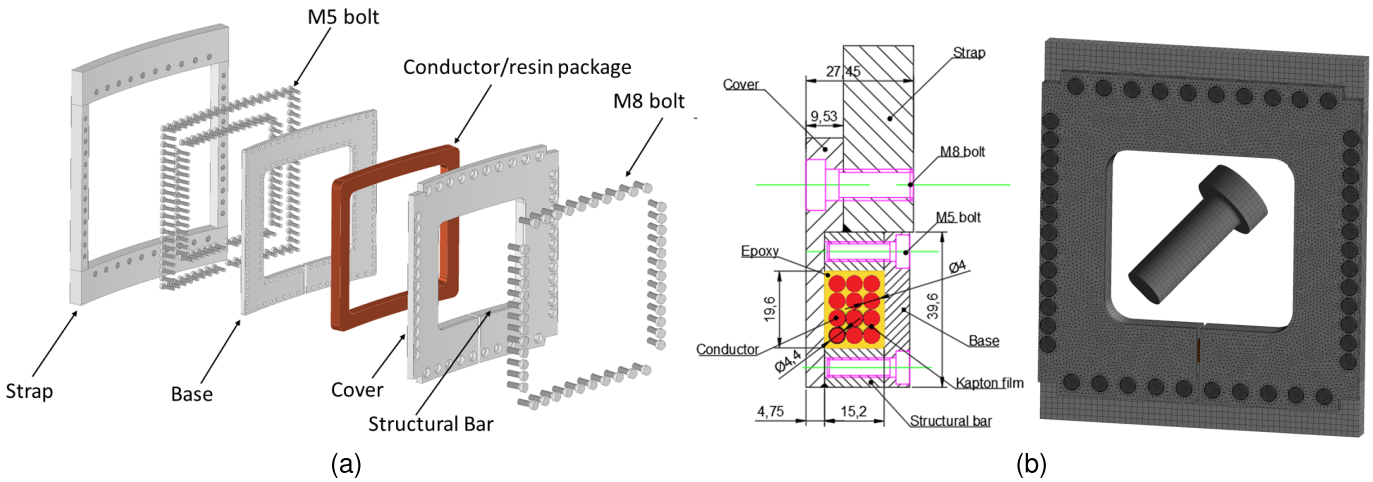

Fig. 2. (a) Exploded view of the IM-coil CAD model. (b) IM-coil cross section and mesh used in ANSYS simulations (1 million elements with 1 mm of the maximum size).

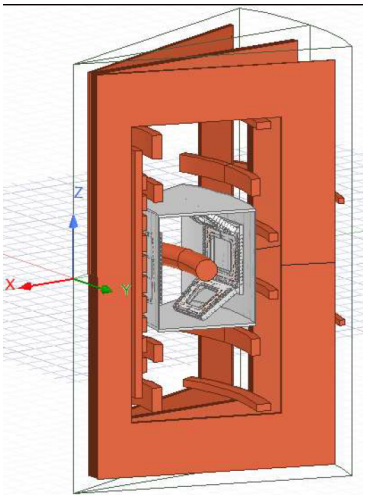

Fig. 3. CAD model used for the Maxwell 3-D simulation.

is adopted, Fig. 3. Note that only half of a toroidal field coil is included in each ends of the computational domain in the toroidal direction (near 0° and 40°). Given this toroidal symmetry, periodic boundary conditions are imposed in the toroidal direction. To provide a toroidal magnetic field of 1.5 T at the R_0 (field envisaged for TCABR after the upgrade), the toroidal field coils must be fed with 66 kA. In these simulations, the poloidal field coils are fed with a specific combination of currents, to create a single-null diverted plasma, and the plasma is modeled by a conductor at R_0 fed with 120 kA, Fig. 3.

A. Electromagnetic Forces

In these simulations, the IM-coil is modeled by a single conductor carrying 2 kA_{dc} × 12 turns = 24 kA-turn, which causes an approximately uniform force per unit volume of about 1×10^8 N/m^3 in the coil vertical legs, Fig. 4. Note that, in conventional aspect ratio tokamaks, such as TCABR, the toroidal magnetic field is about five–ten times higher than the poloidal field. Therefore, the forces in the vertical legs are much stronger than those in the horizontal ones.

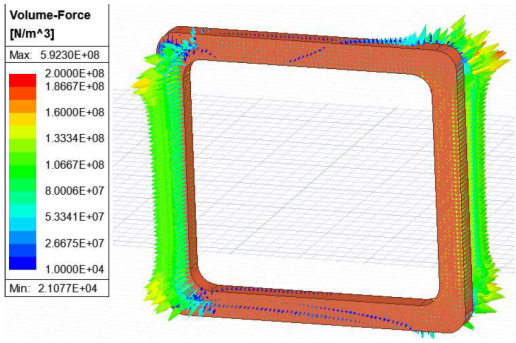

Fig. 4. Electromagnetic force density distribution in the IM-coil conductor.

B. Ohmic Losses

The electromagnetic simulations also allow to calculate the ohmic losses within the coil conductors. For that, however, a new simulation was carried out, where only the wires (12 turns) were modeled and all other CAD components (resin, casings, mechanical supports etc.) were neglected, i.e., the wires heat up adiabatically. For these simulations, the wires were simplified to a square cross section with the same area as the original circular cross section wires. Each turn was fed with 2 kA and the copper electrical resistivity was considered constant and equal to $\rho = 2.57 \times 10^{-8}$ Ω·m during the simulation (no temperature dependence). This value corresponds to the average value of ρ for a range of temperature variation $\Delta T = 220$ °C. The ohmic losses per unit volume found within the wires during these simulations were approximately homogeneous and about 6.5×10^8 W/m^3, Fig. 5.

IV. Transient Thermal Analysis

With the ohmic losses within the coil wires calculated (previous section), the temporal evolution of the temperature distribution within the coil components was calculated using ANSYS' Transient Thermal module. In these simulations, the IM-coils were set to operate for 1 s, during which the ohmic losses make the temperature increase almost adiabatically. After that, the IM-coils cool down for 15 min as heat diffuses

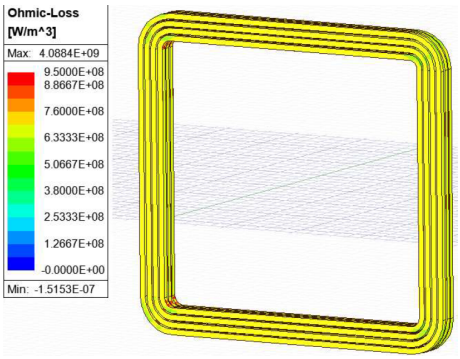

Fig. 5. Ohmic losses in the IM-coil conductor.

from the wires through the epoxy resin to the casing, bolts, and straps. This 15-min cycle of the IM-coils is given by the time required for TCABR to be ready for the next plasma discharge/experiment. The period of 1 s for the operation of the coils at full power was chosen to be slightly smaller than the duration of the plasma current flat top in TCABR after the upgrade, which is envisaged to be $\leq$1.2 s.

In this transient thermal analysis, a CAD model representing the epoxy resin between the wires is combined with the CAD model used for the wires in the electromagnetic analysis. The Kapton insulation layer of 0.2 mm around the wires, however, was neglected in the modeling as its effect on the thermal properties of the whole package is expected to be negligible in comparison with that imposed by the epoxy resin. These simulations also assume that heat can be lost via gray body radiation. As a boundary condition for the radiative losses, the environment temperature was set to 30 °C and a constant gray body emissivity of 0.5 was applied to all external faces of all stainless-steel components.

The simulations show that the maximum temperature within the wires after 2 h of operation (eight discharges) can be as high as about 250 °C, which is the maximum temperature supported by the epoxy resin, Fig. 6. The maximum temperature within the casing and the M8 bolts after the same 2 h of operation is found to be about 110 °C and 90 °C, respectively. These values of temperature occur at $t = 6308$ s, which corresponds to a time immediately after the last of these eight discharges. The temperature distribution within the wires at that particular time can be seen in Fig. 7 while the temperature distribution within the casing and the M8 bolts can be seen in Fig. 8.

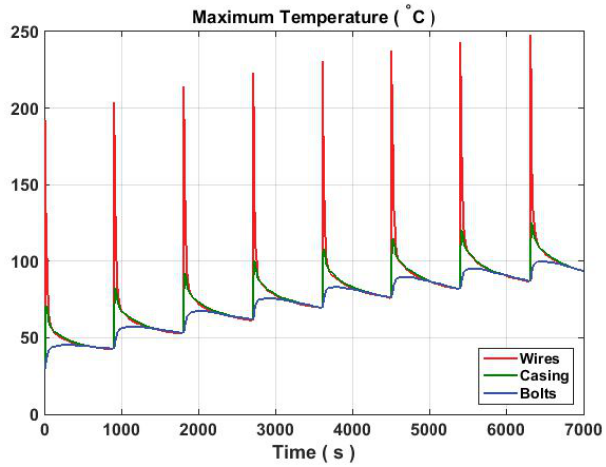

Fig. 6. Temporal evolution of the maximum temperature within the wires (red), casing (green), and M8 bolts (blue).

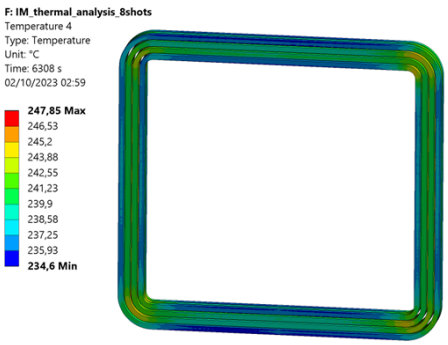

Fig. 7. IM-coil wires temperature distribution immediately after the last of the eight discharges simulated.

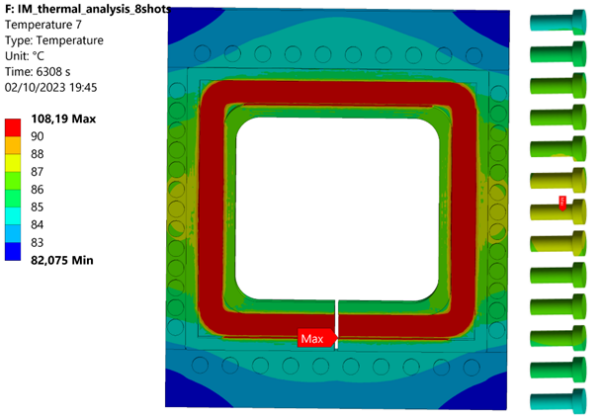

Fig. 8. Temperature distribution on the IM-coil casing and on M8 bolts along the vertical legs immediately after the last of the eight discharges simulated.

V. Mechanical Analysis

A. Boundary Conditions

The static mechanical analysis aims to estimate stresses under which the IM-coils will be subject to, and the corresponding deformation of the coil casing, due to both electromagnetic and thermal loads. These loads are transferred to the stainless-steel casing through contact pairs between the surfaces of the different components of the system. In these simulations, a frictional contact coefficient $\mu = 0.2$ was used between the copper wires and the stainless-steel casing. For all surfaces that are joined by welding, a bonded contact was used. For the coil cover and the straps, a frictional contact coefficient $\mu = 0.2$ was applied. The same sort of contact was applied between the M8 bolts and the coil cover. However, a bonded contact was used between the M8 bolt's bodies and their respective holes in the straps. It is also important to note that the thermal expansion of the coil cover, caused by the temperature increase and temperature gradients, reduces the initial radial gaps of 0.5 mm between the bolts' bodies and their respective holes in the coil cover. This change in the contact status between these surfaces is an additional non-linearity source in the analysis.

TABLE I
ALLOWABLE STRESSES AND TEMPERATURE LIMITS

Criterion	Stress (MPa)
ASME criterion (145 °C)	115
ITER IVC (200 °C)	95
Safety factor n = 3 (200 °C)	73

The CAD model used in these simulations is composed of the straps, the coil base, the conductor, the coil cover, and the M8 bolts used to fasten the coil to the straps. The M5 bolts used to attach the base plate to the structural bars were excluded from this simulation.

Since the straps will be welded on the wall of the vacuum vessel, a fixed support condition was used in all the nodes of this surface. Additionally, a pretension of 1 kN in all the bolts was considered. The standard element types used in the analysis were hexahedrons and tetrahedrons. The average score of these ANSYS' computational mesh was 0.8.

B. Allowable Stress Criteria

In this work, three criteria were used to establish the allowable equivalent von Mises stress levels for the IM-coil casings: 1) the ASME division *D* criterion for pressure vessel [9]; 2) the ITER design of the in-vessel components criterion [10], [11], [12], [13], [14], [15], [16], [17], [18]; and 3) a safety factor $n = 3$ for the 316L yielding stress ($Sy = 220$ MPa) was imposed, Table I.

As the distance between the graphite protection tiles and the coil casing will be about 1 mm, the criterion used for the coil casing maximum deflection was to limit it to 100 μm. It must be stressed that this is a fairly conservative criterion since the elastic behavior of the vacuum vessel was not considered in this analysis. Note that according to the boundary conditions assumed in these structural analyses, the coil casing is rigidly attached to the vacuum vessel straps.

C. Results

The maximum von Mises stress found in these simulations is about 62 MPa, which occurs in the M8 bolts, while the maximum stress in the coil casing, which occurs in the M8 bolts used to fasten the vertical leg to the straps, is around 33 MPa, Fig. 9. The simulations also show that the maximum deformation is about 17 μm, Fig. 10.

VI. DISCUSSION OF THE RESULTS

The transient thermal analysis presented in Section IV shows that the maximum temperature in the 316L mechanical casing and in the M8 bolts was below the temperature limits presented in Table I. However, the maximum temperature within the wires was about 250 °C, which is the maximum temperature supported by the epoxy resin. Therefore, the coils can not be operated for periods longer than about 2-h, unless the operation cycle takes longer than the 15 min considered here.

Fig. 9 shows that the critical components of the IM-coil are the M8 bolts, used to fasten the vertical legs on the straps. Additional simulations show that the maximum stress is predominantly caused by electromagnetic forces (60 MPa due to electromagnetic loads only and 62 MPa due to both electromagnetic and thermal loads). This occurs because the initial gaps between the holes and the bolts allow for an expansion of the coil cover without causing contact stresses.

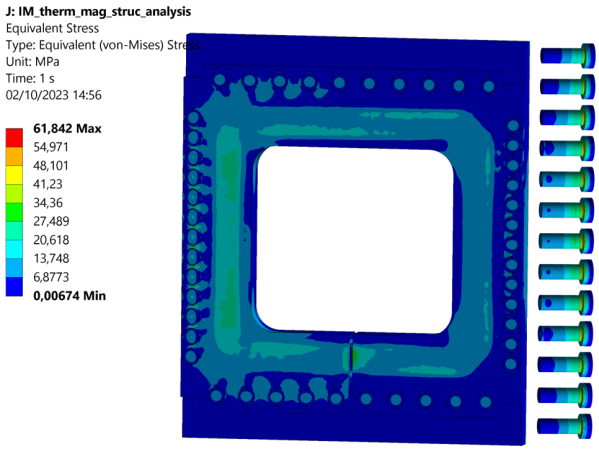

Fig. 9. Stress distribution within the IM-coil casing and M8 bolts along the vertical legs immediately after the last of the eight discharges simulated.

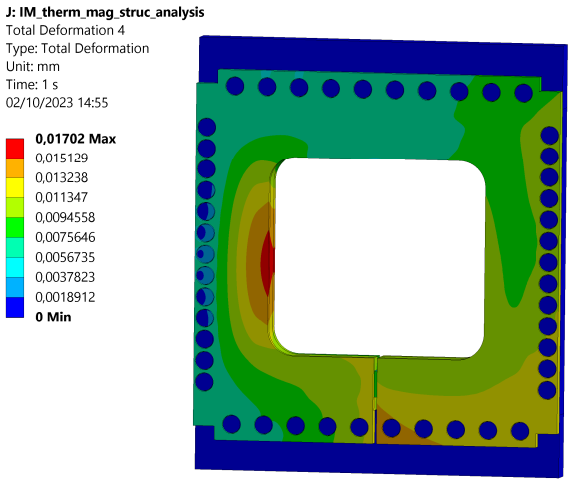

Fig. 10. Deformation distribution within the IM-coil casing immediately after the last of the eight discharges simulated.

The maximum observed stress in Fig. 9 is lower than the allowable stresses presented in Table I, thus the three criteria are satisfied. The total deformation on the IM-coil is caused by temperature gradients, thermal expansion, and electromagnetic forces, Fig. 10. It can be observed that the maximum deformation is about 17 μm, which is lower than the desired allowable deformation.

VII. CONCLUSION

This work presents a feasibility study for the installation of a set of RMP coils inside the TCABR vacuum vessel. In this study, a series of multiphysics, finite element simulations, using the ANSYS software, of the electro-thermal-mechanical stresses within the coil (wires, casing, and bolts) were carried out. Additional components that will also be installed within the TCABR vacuum vessel during the upgrade, such as the

graphite protection tiles and plasma diagnostics, had to be considered in the mechanical design.

The simulations focused of the extreme operation scenario, in which the IM-coils are fed with 24 kA-turn and are operated over 1 s followed by a 15 min interval to the next discharges. After eight cycles (1 s of operation with 15 min of cool down), which correspond to about 2 h of operation, a transient thermal analysis was carried on. The simulations show that, after the last of these eight discharges, the maximum temperature within the wires was about 250 °C, which is the maximum temperature supported by the epoxy resin. This means that the coils can not be operated longer than about 2 h in this operation cycle regime, unless a longer than 15 min is considered for the coils to cool down sufficiently. The structural analysis of the IM-coil mechanical casing considered temperature gradients, thermal expansion, and electromagnetic forces. The estimated maximum stress within the coil components did not exceed the allowable stresses established by three different criteria, showing that the presented design for the mechanical casing is feasible. The analysis performed in this work demonstrated that the IM-coils also met other imposed criteria, such as the one related to maximum deflection. It is important to observe that the M8 bolts are the critical components of the coil.

Future analyses will focus on feasibility studies regarding the installation of the other envisaged TCABR in-vessel coils, i.e., the IU- and IL-coils, located on the LFS, and the CP-coils, located on the HFS.

ACKNOWLEDGMENT

The authors would like to thank the Institute Mauá of Technology, São Paulo, Brazil, for providing the ANSYS software licenses and the computational resources used in this work.

REFERENCES

[1] J. Severo et al., "Temporal behaviour of toroidal rotation velocity in the TCABR tokamak," *Nucl. Fusion*, vol. 49, no. 11, 2009, Art. no. 115026, doi: 10.1088/0029-5515/49/11/115026.

[2] P. B. Snyder et al., "Edge localized modes and the pedestal: A model based on coupled peeling–ballooning modes," *Phys. Plasmas*, vol. 9, no. 5, pp. 2037–2043, May 2002.

[3] P. B. Snyder et al., "The EPED pedestal model and edge localized mode-suppressed regimes: Studies of quiescent H-mode and development of a model for edge localized mode suppression via resonant magnetic perturbations," *Phys. Plasmas*, vol. 19, no. 5, May 2012, Art. no. 056115.

[4] T. E. Evans et al., "Edge stability and transport control with resonant magnetic perturbations in collisionless tokamak plasmas," *Nature Phys.*, vol. 2, no. 6, pp. 419–423, Jun. 2006.

[5] T. E. Evans, "Resonant magnetic perturbations of edge-plasmas in toroidal confinement devices," *Plasma Phys. Controlled Fusion*, vol. 57, no. 12, Nov. 2015, Art. no. 123001.

[6] A. O. Santos et al., "Development of high-current power supplies for the TCABR tokamak," *Fusion Eng. Design*, vol. 159, Oct. 2020, Art. no. 111698.

[7] F. Salvador, G. Canal, D. Orlov, A. Bouzan, and M. Kot, "Design of an innovative set of RMP coils for TCABR," *Bull. Amer. Phys. Soc.*, vol. 66, no. 63, pp. 11–47, Nov. 2021.

[8] N. M. Ferraro and S. C. Jardin, "Calculations of two-fluid magneto-hydrodynamic axisymmetric steady-states," *J. Comput. Phys.*, vol. 228, no. 20, pp. 7742–7770, Nov. 2009.

[9] A. Boiler, *ASME Boiler and Pressure Vessel Code: An International Code*. New York, NY, USA: American Society of Mechanical Engineers, 2021.

[10] I. Zatz, *Structural Design Criteria for ITER In-vessel Components (SDC-IC) Appendix D In-vessel Coils (IVC)*, document ITERD3WK338, 2012.

[11] Y. Cen et al., "Stress and thermal analysis of the in-vessel RMP coils in HL-2M," *Plasma Sci. Technol.*, vol. 15, no. 9, pp. 939–944, Sep. 2013.

[12] S. Wang et al., "Thermo-mechanical analysis of RMP coil system for EAST tokamak," *Fusion Eng. Design*, vol. 89, nos. 7–8, pp. 991–995, Oct. 2014.

[13] S. Zhang et al., "Mechanical analysis and optimization of ITER upper ELM coil & feeder," *Plasma Sci. Technol.*, vol. 16, no. 8, pp. 794–799, Aug. 2014.

[14] S. Zhang, Y. Song, L. Tang, Z. Wang, X. Ji, and S. Du, "Electromagnetic–thermal–structural coupling analysis of the ITER edge localized mode coil with flexible supports," *Plasma Sci. Technol.*, vol. 19, no. 5, Mar. 2017, Art. no. 055601.

[15] S. Zhang, Y. Song, Z. Wang, E. Daly, and M. Kalish, "Mechanical analysis for ITER upper ELM coil," in *Proc. IEEE 25th Symp. Fusion Eng. (SOFE)*, Jun. 2013, pp. 1–5.

[16] S. W. Zhang et al., "Structural analysis and optimization for ITER upper ELM coil," *Fusion Eng. Design*, vol. 89, no. 1, pp. 1–5, Jan. 2014.

[17] C. Hao, M. Zhang, Y. Ding, B. Rao, Y. Cen, and G. Zhuang, "Stress and thermal analysis of the in-vessel resonant magnetic perturbation coils on the J-TEXT tokamak," *Plasma Sci. Technol.*, vol. 14, no. 1, pp. 83–88, Jan. 2012.

[18] A. W. Brooks, Y. Zhai, E. Daly, M. Kalish, R. Pillsbury, and A. Khodak, "Thermal and structural analysis of the ITER ELM coils," in *Proc. IEEE 25th Symp. Fusion Eng. (SOFE)*, Jun. 2013, pp. 1–6.